Ahlborn, M., Haberzettl, T., Wang, J., Henkel, K., Kasper, T., Daut, G., Zhu, L., Mäusbacher, R. (2017): Synchronous pattern of moisture availability on the southern Tibetan Plateau since 17.5 cal. ka BP - the Tangra Yumco lake sediment record. - *Boreas*, *46*, 2, pp. 229—241.

DOI: http://doi.org/10.1111/bor.12204

Synchronous pattern of moisture availability on the southern Tibetan Plateau since 17.5 cal. ka BP – the Tangra Yumco lake sediment record

MARIEKE AHLBORN, TORSTEN HABERZETTL, JUNBO WANG, KAROLINE HENKEL, THOMAS KASPER, GERHARD DAUT, LIPING ZHU AND ROLAND MÄUSBACHER

Ahlborn, M., Haberzettl, T., Wang, J., Henkel, K., Kasper, T., Daut, G., Zhu, L. & Mäusbacher, R.: Synchronous pattern of moisture availability on the southern Tibetan Plateau since 17.5 cal. ka BP – the Tangra Yumco lake sediment record. *Boreas.*

A possible asynchronicity of the spatial and temporal moisture availability on the Tibetan Plateau was controversially discussed in recent years. Here we present the first attempt to systematically investigate possible spatial and temporal variations of moisture availability by examining two lakes, Tangra Yumco and Nam Co, on an east-west-transect on the southern Tibetan Plateau using identical proxies for palaeoenvironmental reconstruction. In this study, an independent record from Tangra Yumco was analyzed applying a multi-proxy approach to reconstruct variations in moisture availability since the Lateglacial. Results were subsequently compared to previously published records from Nam Co and additional records from Tso Moriri (northwestern Himalaya) and Naleng Co (south-eastern Tibetan Plateau). Our results show that Tangra Yumco was at least partially ice-covered prior to 17.1 cal. ka BP. A temperature rise after 17.1 cal. ka BP probably resulted in thawing of the permafrost. At 16.0 cal. ka BP moisture availability increased representing an initial monsoonal intensification. Warmer conditions between 13.0 and 12.4 cal. ka BP and cooler conditions between 12.4 cal. ka BP and the onset of the Holocene reflect the Bølling-Allerød and Younger Dryas. At the onset of the Holocene moisture availability rapidly increased, while moisture was highest prior to 8.5 cal. ka BP concurrently with highest temperatures. After 8.5 cal. ka BP the moisture availability gradually decreased and showed only minor amplitude variations. These findings are well in phase with the records from other large lakes likes Nam Co, Tso Moriri, and Naleng Co revealing a synchronous pattern of moisture availability on the southern Tibetan Plateau.

Marieke Ahlborn[+] (marieke.ahlborn@gfz-potsdam.de), Torsten Haberzettl, Karoline Henkel, Thomas Kasper, Gerhard Daut and Roland Mäusbacher, Physical Geography, Institute of Geography, Friedrich Schiller University Jena, Löbdergraben 32, 07743 Jena, Germany; Junbo Wang and Liping Zhu, Key Laboratory of Tibetan Environment Changes and Land Surface Processes, Institute of Tibetan Plateau Research, Chinese Academy of Sciences, Beijing 100101, China

[+] *Present address: Section 5.2: Climate Dynamics and Landscape Evolution, GFZ German Research Centre for Geosciences, 14476 Potsdam, Germany*

In the past decades a possible asynchronicity of moisture availability in monsoonal Asia and on the Tibetan Plateau was thoroughly investigated. Several studies suggested an asynchronous pattern of moisture availability since the Last Glacial Maximum (An *et al.* 2000; He *et al.* 2004; Herzschuh 2006; Mischke *et al.* 2008; Wang *et al.* 2010b; Wischnewski *et al.* 2011; Hudson & Quade 2013). An *et al.* (2000) and Ramisch *et al.* (2016) suggested a non-stationary position of the northern monsoon limit as a cause for a spatial asynchronicity. Mischke *et al.* (2008) discussed small-scale variabilities explaining that local peculiarities like temperature-driven evaporation can outweigh a precipitation increase, thus, resulting in drier conditions at specific sites while other areas are moist. In contrast, other studies rather indicate a synchronous pattern of moisture availability (Feng *et al.* 2006; Chen *et al.* 2008; Dong *et al.* 2010; Mischke & Zhang 2010) with a synchronous development of the Indian and the East Asian monsoon (Dong *et al.* 2010). However, as reliable, continuous records covering the Lateglacial and the Holocene are rare, a holistic picture of variability of moisture availability including spatial and temporal changes, and the impact on the environment is still missing (Herzschuh 2006; Mischke & Zhang 2010).

To investigate past variability of moisture availability on the southern Tibetan Plateau, two lakes along an east-west-transect, including Tangra Yumco and Nam Co (Fig. 1) were recently targeted for palaeoenvironmental studies. Nam Co was thoroughly investigated in recent years (e.g. Daut *et al.* 2010; Mügler *et al.* 2010; Kasper *et al.* 2012, 2013, 2015; Wang *et al.* 2012; Su *et al.* 2013; Doberschütz *et al.* 2014; Yang *et al.* 2014; Wang *et al.* 2015; Zhu *et al.* 2015) and several studies have been conducted in the Tangra Yumco catchment (Kong *et al.* 2011; Long *et al.* 2012; Rades *et al.* 2013, 2015; Miehe *et al.* 2014; Ahlborn *et al.* 2015, 2016; Akita *et al.* 2015; Long *et al.* 2015; Henkel *et al.* 2016). In this study, we present results from an 11.2-m-long lacustrine sediment record from Tangra Yumco. The objectives of this study are to deduce changes in palaeohydrology and palaeoenvironment for the Tangra Yumco area and infer the temporal and spatial moisture availability on the southern Tibetan Plateau by comparison to previously published records using identical proxies from Nam Co (Kasper *et al.* 2015). For an extension of the east-west-transect we have chosen two additional lakes namely Tso Moriri (northwestern Himalaya; for reasons of simplification we refer to southern Tibetan Plateau; Mishra *et al.* 2015) and Naleng Co (south-eastern Tibetan Plateau; Opitz *et al.* 2015) (Fig. 1). Reasons for selection of these lakes were the similar geographical settings like altitude, latitude, and recent monsoonal influence, and the time covered by the records.

Regional setting

Tangra Yumco (30°45'–31°22' N, 86°23'–89°49' E; Fig. 1) is located on the southern Tibetan Plateau at an elevation of 4545 m a.s.l. (Rades *et al.* 2013) with a catchment of 8219 km^2 (Long *et al.* 2012). The Tangra Yumco basin belongs to a north-south-trending graben at the northern slope of the Transhimalaya (Miehe *et al.* 2014). Well-preserved palaeoshorelines are exposed up to ~185 m above the recent lake level (m a.r.l.l.) (Rades *et al.* 2013), whereas poorly-preserved palaeoshorelines are exposed up to >260 m a.r.l.l. indicating extensive lake level changes during the past (Kong *et al.* 2011). Precipitation at Tangra Yumco is dominated by the Indian summer monsoon originating from the south (Miehe *et al.* 2014), while westerly winds prevail during the winter months (Maussion *et al.* 2014). The extrapolated mean annual precipitation is 200–250 mm, the mean temperature in January is -11.4 °C, and the mean July temperature 10.9 °C (Miehe *et al.* 2014).

Tangra Yumco (Fig. 1B) is a brackish lake with a salinity of 8.3‰ covering 818 km² (Long *et al.* 2012). With a water depth of 230 m Tangra Yumco is the deepest lake recorded on the Tibetan Plateau so far (Wang *et al.* 2010a). The lake has a northern and a southern part connected by a bottleneck-like structure (Fig. 1). Two large rivers drain into Tangra Yumco entering the southern part of the lake from the southeast and west. Tangra Yumco lacks an outflow and is currently a terminal lake. Due to its terminal character lake level variations of Tangra Yumco are mainly controlled by precipitation and temperature (evaporation), while the contribution of glaciers is negligible (Rades *et al.* 2013; Biskop *et al.* 2015). Submerged lake level terraces (Akita *et al.* 2015) represent significantly lower lake levels in the past. A connection to the nearby Tanqung Co (about 18 km north of Tangra Yumco) is possible when the lake level of Tangra Yumco reaches an elevation of ~64 m a.r.l.l. (Ahlborn *et al.* 2016). The population in the Tangra Yumco area is sparse and human impact is mainly restricted to pastoralism (Miehe *et al.* 2014).

Material and methods

Field methods and composite profile

Based on the results of hydro-acoustic surveys (Innomar SES-96 light and Lowrance Echosounder HDS 5) coring locations were selected for recovery of sediment cores TAN10/4 and TAN12. In 2010, gravity core TAN10/4 was collected with a total length of 1.62 m in 223 m water depth. In 2012, piston core TAN12 with a total length of 11.5 m was retrieved from 217 m water depth about 2 km south of

core TAN10/4. Due to coring artefacts and the lack of a parallel core, sediment core TAN12 lacks the upper 13 cm of sediment including the sediment-water interface and 17 cm of sediment at the base of each core section that are shown as data gaps in the composite profile (Henkel *et al.* 2016). Cores TAN10/4 and TAN12 were merged to a composite profile using several marker layers in order to replace the upper 13 cm sediment missing in sediment core TAN12 (Henkel *et al.* 2016). The lithological correlation of both cores is supported by magnetic susceptibility and Ti profiles (Henkel *et al.* 2016).

Non-destructive laboratory methods

Until further processing all cores were stored in darkness at +4 °C. The cores were split and subjected to an initial core description including high-resolution imaging and magnetic susceptibility logging (Bartington MS 2E point sensor). The split cores were XRF scanned with radiographic image documentation (ITRAX Corescanner; Croudace *et al.* 2006). XRF scanning was conducted with 2 mm resolution for sections TAN12/1 to 7 and with 0.2 mm resolution for sections TAN12/8 to 11 and TAN10/4 using a molybdenum tube set to 55 kV and 40 mA. Exposure time was 10 s for all sections of core TAN12 and 4 s for TAN10/4. To compensate for different exposure times, element peak area (pa) values were normalized to the exposure time applied and subsequently to kilo counts per second (kcps). For principle component analysis (PCA), normalized values were z-transformed. Since core TAN10/4 was obtained from a different location within Tangra Yumco, overlapping XRF data of core TAN10/4 were plotted on a separate x-axis and adjusted to the data of core TAN12. Elements with pa >100 were considered as reliable and used for interpretation (Brunschön *et al.* 2010; Kasper *et al.* 2012).

Destructive laboratory methods

Double-L-channels (Nakagawa 2007) were taken from all sections and continuously sub-sampled in 1 cm intervals for grain size and geochemical analyses. For grain size analysis, samples were pretreated with H_2O_2 10% p.a. and HCl 10% p.a. to dissolve organic compounds and carbonates. Dispersion of the grains was ensured using sodium pyrophosphate ($Na_4P_2O_7$•10 H_2O, 0.1 mol L^{-1}) and samples were shaken for 2 h. Grain size distribution was measured (LS 13320 Beckmann Coulter) in seven cycles of 60 s each and the first reproducible signal was used for interpretation applying the Frauenhofer optical model and a modified version of Gradistat 4.2 (Blott & Pye 2001) for statistical calculations.

Samples for geochemical analysis were freeze-dried and ground (<40 µm). Scaling before and after the freeze-drying procedure defined the water content of the sediments. Core TAN10/4 was

sampled in a 1 cm resolution, while analyses on core TAN12 were performed in a varying resolution of 1 to 10 cm depending on lithological variations. All samples were subjected to analyses of total carbon (TC), total sulfur (TS), and total nitrogen (TN) using an elemental analyzer (Vario El Cube). Carbonates were dissolved with HCl 30% p.a. prior to the measurements of total organic carbon (TOC) with the same device. Total inorganic carbon (TIC) was calculated as the difference of TC and TOC and atomic C/N ratios were calculated.

Event corrected composite depth (ECCD)

Possible event-related deposits (ERD) resulting from deposition of relocated sediment material were identified based on lithology, radiographic images, magnetic susceptibility, Ti values, grain size data, and water content. For final interpretation, ERDs and corresponding data were excluded from the composite profile. The event corrected record is presented on an artificial depth axis, the so-called 'event corrected composite depth' (ECCD) that is strictly used hereafter (Henkel *et al.* 2016).

Chronology

Due to the lack of plant macro-remains bulk sediment samples from sediment cores TAN10/4 and TAN12 were used for radiocarbon dating. The chronology of core TAN10/4 is based on five radiocarbon ages on bulk sediment samples and one age obtained from a wood fragment of terrestrial origin, while 22 bulk sediment samples were obtained from sediment core TAN12 (Beta Analytics Inc., USA). To estimate a potential reservoir effect the sediment-water interface of sediment core TAN10/4 and a modern water plant were dated. The age of the modern water plant was used as reservoir effect and subtracted from all conventional radiocarbon ages, except the age obtained from the terrestrial wood sample. After reservoir correction, the calibrated ages and 2σ errors were calculated with the online version of Calib 7.0 (Stuiver & Reimer 1993) applying the IntCal13 dataset (Reimer *et al.* 2013). To establish the chronology, the reservoir-corrected and calibrated radiocarbon ages were linearly interpolated (Haberzettl *et al.* 2015; Henkel *et al.* 2016).

Lithological and geochemical results on an event-corrected composite depth scale

The composite profile of the parallelized core sections has a total length of 11.2 m, while the event-corrected ECCD length is 848 cm (Fig. 2; Henkel *et al.* 2016). Sediments in core TAN12 are generally

laminated silts. Black sandy layers occur exclusively below 711 cm ECCD. Colors are dark gray with faint lamination of millimeter-scale below 625 cm ECCD. Between 625 and 575 cm ECCD, sediments are gray but overall lighter with clearly defined lamination of submillimeter scale. Above 575 cm ECCD, sediments are yellowish brown to brownish gray with light gray to gray laminae of subcentimeter- to centimeter-scale. The lithology of core TAN10/4 revealed mainly laminated sediments with varying laminae thicknesses of submillimeter- to millimeter-scale and yellowish brown, brownish gray to blackish colors.

In both cores, laminated sediments are intercalated by discrete, normally graded, homogenous sediment sections with varying thickness of centimeter- to decimeter-scale. These sediment sections are associated with higher magnetic susceptibility and Ti values, higher density as shown by radiographic images, and lower water content (Henkel *et al.* 2016). Earlier studies showed that such discrete sediment sections represent event-related deposits (ERDs) intercalating the continuous background sedimentation (Sletten *et al.* 2003; Ahlborn *et al.* 2015; Akita *et al.* 2015). In total, seventeen ERDs were identified and removed from the sedimentary record (Fig. 3; Henkel *et al.* 2016).

For correlation of cores TAN10/4 and TAN12 prominent sedimentary structures were used as marker layers. One, about 1-cm-thick dark gray silty layer in the depth of 83 cm in core TAN10/4 and 64 cm depth in core TAN12 and three additional discrete, homogenous layers served as anchor points for core correlation. This lithological correlation is refined by the patterns of magnetic susceptibility and Ti (Henkel *et al.* 2016).

Ti is positively correlated with K, Fe, and Rb ($R_{Ti:K}$ = 0.69, $R_{Ti:Fe}$ = 0.69, and $R_{Ti:Rb}$ = 0.59). Sr and Ca show a correlation coefficient of $R_{Ca:Sr}$ = 0.40. Results of the PCA show that the principle components 1 (PC1) and 2 (PC2) account for 77.48% of the total variance (Fig. 3). PC1 yields high values for K, Ti, Fe, and Rb and accounts for 63.06% of the total variance while PC2 accounts for 14.43% and basically represents Sr (Fig. 4). The remaining PCs have only low account on the total variance with <10% each. PC1 is rapidly increasing at 625 cm ECCD showing a minor peak at 594–558 cm ECCD, variable values at 456–355 cm ECCD, and remains relatively stable above 355 cm ECCD. Between 456 and 297 cm ECCD Ca is strongly anti-phased correlated with PC1 as the correlation coefficient is $R_{Ca:PC1}$ = -0.83 (Fig. 3).

TIC, TOC, TN, and C/N data are positively correlated (Fig. 3). TIC values range from 0.66–6.56% and resemble the Ca pattern with a correlation coefficient of $R_{TIC:Ca}$ = 0.74. TOC and TIC are positively correlated with a correlation coefficient of $R_{TOC:TIC}$ = 0.30. TOC content is generally low, varies

from 0.1–1.1%, and is highly correlated to TN with $R_{TOC:TN}$ = 0.93. TOC and TN reveal lowest values in the entire core below 711 cm ECCD, highest values at 711–625 cm, lower but generally stable values at 625–594 cm, and a minor peak 594–558 cm ECCD. Values are markedly reduced at 558–456 cm ECCD, increasing thereafter, and culminating in a broad maximum at 418–383 cm ECCD. TOC and TN are relatively stable above 297 cm. C/N ratios vary from 3.9–10.1 only exceeding 10 at 711–625 cm ECCD (Fig. 3). Mean relative errors are 0.6% for TC, 11.2% for TS, 9.3% for TN, and 4.6% for TOC.

The arithmetic mean of the grain size data varies between 7.3–225.1 µm (Fig. 3). Large modes between 120 and 220 µm only occur below 711 cm in black sandy layers associated with maximum mean values (220 µm). These black sandy layers have an almost unimodal distribution and are very well sorted (Fig. 5). Gravel (>2 mm) is recorded at 768 and 750 cm ECCD (Fig. 3). Above 711 cm ECCD mean values decrease down to 12 µm followed by a sharp increase to 30 µm at 625 cm ECCD, and relatively stable values thereafter. A drop to 8 µm occurs at 558 cm ECCD, followed by a maximum of 56 µm at 418–387 cm ECCD. Values decline down to 9 µm until 297 cm ECCD showing minor variations thereafter (Fig. 3).

Chronology

As Tibetan lakes commonly suffer from reservoir effects (Mischke *et al.* 2013) a thorough assessment of the reservoir effect is a precondition for establishing valid radiocarbon chronologies. According to the age of the modern water plant Tangra Yumco holds a reservoir effect of 2070±30 years consistent with the age of the sediment-water interface of core TAN10/4 of 2140±30 years. However, since both ages are very similar but the sediment-water interface bulk sediment sample might already integrate over several years, the usage of the age of the modern water plant is more appropriate (Henkel *et al.* 2016). The reservoir effect is further verified by OSL ages measured on sediments of core TAN10/4. These OSL ages yield an age offset of approximately 2000 years relative to the uncorrected radiocarbon ages (Long *et al.* 2015) supporting the assumption of a constant reservoir effect over time (Henkel *et al.* 2016).

A contamination of dating samples can occur by reworking of fine organic matter containing 'old carbon' or a hardwater effect of the hostwater of living plants biasing the radiocarbon ages (Haberzettl 2015; Haberzettl *et al.* 2015). Outliers or biased ages were defined as ages that are too old in comparison to neighboring ages in stratigraphic order and considerably alter the sedimentation rate

without any corresponding changes in the lithology. Such outliers were excluded from the chronology (Henkel *et al.* 2016). Finally, six ages had to be rejected as outliers and the median of the 2σ distribution of the 18 youngest ages in stratigraphic order was used to establish the chronology. The event-corrected composite record covers the past 17.5 cal. ka BP. The sedimentation rate is 3.6 mm a^{-1} below 711 cm ECCD (17.1 cal. ka BP) and with <0.6 mm a^{-1} significantly lower above (Fig. 2; Henkel *et al.* 2016).

In the past years, studies emphasized the necessity of validating incremental chronologies using independent dating methods like palaeomagnetic secular variations (PSV) (e.g. Stanton *et al.* 2010). Several studies demonstrated the successful application of PSV on Tibetan lakes to further verify the radiocarbon based chronologies (e.g. Kasper *et al.* 2012; Ahlborn *et al.* 2015; Haberzettl *et al.* 2015; Lockot *et al.* 2015; Ramisch *et al.* 2016). PSV of the Tangra Yumco record is in good agreement with the Lake Baikal record, the East Asian PSV stack, and the geomagnetic field model for the past 15.9 cal. ka BP (length of PSV record from Tangra Yumco) which supports the reliability of the presented radiocarbon chronology (Henkel *et al.* 2016).

Palaeoenvironmental reconstruction of Tangra Yumco

The hydrological development of Tangra Yumco can be subdivided into several phases. The occurrence of sandy layers (modes 120 and 220 µm) and gravels restricted to the phase from 17.5 to 17.1 cal. ka BP (848–711 cm ECCD) suggests unique palaeoenvironmental conditions at Tangra Yumco (Fig. 3). An end member modelling approach on sediments from various Tibetan lakes including Tangra Yumco showed that grain size distributions with modes between 90 and 250 µm represent 'aeolian sands' (Sun *et al.* 2002) derived from local sources that move by rolling and saltation (Fig. 5; Dietze *et al.* 2014). Similar findings were presented by Pye & Tsoar (2009) revealing that unimodal and well sorted sediments in the range of 100 to 300 µm are associated with aeolian processes and move by saltation (Fig. 5), while grains >90 µm might even be transported in short-term suspension. In modern surface sediments from lake Donggi Cona (north-eastern Tibetan Plateau) these 'aeolian sands' move by rolling and/or saltation on a frozen lake. A (at least partial) frozen lake surface is therefore required to transport these 'aeolian sands' to distal positions of the lake like the coring location in Tangra Yumco (Dietze *et al.* 2012). This aeolian transport process is probably driven by strong surface winds from westerly and northerly directions during fall and spring seasons (Dietze *et al.* 2014). Alternatively, sediments trapped in the frozen lake surface could also be transported by ice-rafting (Dietze *et al.* 2014) which at least

applies to the gravels found in the Tangra Yumco record as they are too coarse for aeolian transport. Fluvial sediments, in turn, have a multimodal character with coarse modes of typically 200 to 400 µm (Sun *et al.* 2002). Therefore, fluvial transport processes are unlikely to be responsible for deposition of these unimodal sandy layers. The occurrence of the sandy layers might also explain the high sedimentation rate as these layers do not represent the continuous background sedimentation but rather a seasonal accumulation of sediment or even single events.

Reasons for the termination of the deposition of these sandy layers and gravel might be either the lack of an ice-covered surface or a change in wind direction or strength. However, our data do not indicate any changes in wind direction or strength although it could potentially have happened. In contrast, there are indications for a change in temperatures. C/N ratios are typically low in non-vascular aquatic plants with values between 4 and 10 and higher in terrestrial vascular plants with values >20 and thus indicative for the origin of organic matter (TOC) in the sediments (Kemp *et al.* 1977; Krishnamurthy *et al.* 1986; Meyers & Ishiwatari 1993). As C/N ratios before 17.1 cal. ka BP are <10, pointing to an autochthonous origin of the TOC, the TOC content mainly reflects changes in the autochthonous production which has been linked to temperature variations (Zhu *et al.* 2008; Kasper *et al.* 2012). The same interpretation applies for Ca and TIC which are positively correlated to TOC and hence are indicative of autochthonous carbonate production controlled by temperature variations. Ca and TIC can, alternatively, be governed by the input of detrital carbonates but should than be correlated to PC1 which is not the case in the Tangra Yumco record. Other studies showed that Ca can act as a lake level indicator with higher Ca when the lake level is low due to concentration effects. In that case, Ca and PC1 would show a strong anti-phased correlation (Kasper *et al.* 2012) which also does not apply for the Tangra Yumco record. Therefore, we consider Ca as indicative of autochthonous production and temperature variations. The TOC and Ca contents before 17.1 cal. ka BP are lowest in the record what might reflect coldest conditions. So probably increasing temperatures and a lack of ice cover caused the termination of the deposition of the sandy layers.

The phase from 17.1 to 16.0 cal. ka BP (711–625 cm ECCD) is characterized by rapidly increasing and highest TOC contents in the record, while grain size and PC1 values remain low. Increasing Ca and, more pronounced, TIC content represents higher autochthonous production and elevated temperatures. Probably Tangra Yumco might have been a very shallow lake that responded quickly to changes in temperature reflected in the elevated TIC and Ca contents. The high TOC content corresponds to higher C/N ratios with values >10 representing highest values in the sedimentary record

and indicating a terrestrial origin of the TOC (Fig. 3). As demonstrated in previous studies, Ti can be considered as indicator for allochthonous clastic input into a lake that is often transported fluvially by enhanced surface runoff (Haberzettl *et al.* 2009; Kasper *et al.* 2012; Doberschütz *et al.* 2014). High correlations of Ti with K, Fe, and Rb indicate that these elements also represent the allochthonous clastic input (Brunschön *et al.* 2010). As these elements have a high load on PC1, it reflects the allochthonous clastic input by surface runoff that is persistently decreasing from 17.1 to 16.0 cal. ka BP (Fig. 4). However, determination of the driver of the allochthonous clastic input is not straightforward as precipitation and glacial meltwater come into question. In Tangra Yumco glacial meltwater likely contributed to the hydrological budget in the Late Pleistocene (Rades *et al.* 2013). However, the extent of the contribution of meltwater remains unknown. So for the Late Pleistocene we preliminarily refer to surface runoff by using PC1. Decreasing surface runoff from 17.1 to 16.0 cal. ka BP is also indicated by fining grain sizes. A grain size record from Lake Daihai (Inner Mongolia) showed that the median grain size decreases coeval with reduced surface runoff and increases with enhanced surface runoff. In that study, the surface runoff was linked to monsoonal precipitation (Peng *et al.* 2005). However, the high input of terrestrial TOC with concurrent decreasing surface runoff is difficult to explain. We speculate that a further increase in temperature, as suggested by TIC and Ca, terminated the deposition of sandy layers and caused a thawing of the permafrost releasing large amounts of terrestrial TOC from the topsoil then available for erosion, transport, and deposition in the lake.

At 16.0 cal. ka BP (625 cm ECCD) the allochthonous clastic input rises as indicated by rapid increases in grain sizes and PC1, while concurrently the TOC, C/N, Ca, and, more pronounced, the TIC content declines. The rise of the allochthonous clastic input points to enhanced surface runoff either by more precipitation or glacial meltwater what would suggest that temperatures were further rising. The rapid return to lower TOC and C/N reflects that the input of terrestrial TOC decreased. Tangra Yumco might have been a very shallow lake before 16.0 cal. ka BP and the rising lake levels, due to enhanced surface runoff, might have increased the distance from the coring location to the shore consequently reducing the delivery and deposition of terrestrial TOC from the catchment. The increasing water volume might have altered the water chemistry and decreased the carbonate production. Submerged lake level terraces (Akita *et al.* 2015) might possibly support the hypothesis of a very shallow lake. Apparently, the environmental conditions changed significantly towards moister conditions at 16.0 cal. ka BP (Fig. 3).

Between 16.0 and 13.0 cal. ka BP (625–569 cm ECCD) the TOC content remains relatively stable with corresponding low C/N ratios indicating low autochthonous production and rather low but

319 stable temperatures. This interpretation is supported by relatively stable but low TIC and Ca contents
320 (Fig. 3).

321 Between 13.0 and 12.4 cal. ka BP (569–456 cm ECCD) TOC, grain sizes, and PC1 increases
322 followed by a decrease between 12.4 and 11.4 cal. ka BP (539–456 cm ECCD). As C/N ratios are still
323 <10, TOC reflects variations in temperatures with higher temperatures between 13.0 and 12.4 cal. ka BP
324 and cooler conditions prior to the onset of the Holocene contemporary to the Northern Hemisphere
325 Younger Dryas chronozone. Similarly, the surface runoff, as indicated by PC1, is enhanced before
326 12.4 cal. ka BP and lower subsequently. Variability of the grain sizes is too high to reveal a general trend
327 possibly suggesting that the environmental conditions were unstable in that phase (Fig. 3).

328 After 11.4 cal. ka BP (456 cm ECCD) TOC, grain sizes, and PC1 considerably increase. TOC
329 reaches the highest values at 9.2 cal. ka BP (385 cm ECCD) and since the C/N ratio is constantly <10,
330 TOC reflects the autochthonous production and therefore a temperature peak with a subsequent drop
331 in temperatures. According to PC1 the surface runoff significantly declines after 10.8 cal. ka BP (426 cm
332 ECCD), while grain sizes further increase indicating rising surface runoff with a peak almost concurrently
333 to the peak in temperature. Assuming that PC1 is biased and the grain size data show the actual
334 development of the surface runoff, two possible scenarios can resolve this apparent contradiction
335 between grain size and PC1 data. A strong anti-phased correlation between Ca and PC1 might point to
336 a dilution effect of PC1. High temperatures, as they are suggested by TOC, could have enhanced the
337 autochthonous carbonate production and the carbonate dilutes the allochthonous clastic input leading
338 to a decrease in PC1. Alternatively, due to a significantly higher lake level less allochthonous clastic
339 material might have reached distal parts (coring location) of the lake. This might have caused a decline
340 in PC1 although the surface runoff was still similar. A significantly higher lake level is also confirmed by
341 a Holocene lake level reconstruction from Tangra Yumco (Fig. 6) based on optically stimulated
342 luminescence (OSL) ages of exposed lacustrine sediments and recalculated cosmogenic nuclide ages
343 of beach terraces. This lake level reconstruction indicates a rising lake level at 10.5 ka, a lake level
344 highstand prior to 8.5 ka, and falling lake level thereafter (Ahlborn *et al.* 2016). These results are well in
345 phase with the grain size data that reveal increasing precipitation until approximately 9.2 cal. ka BP and
346 might probably suggest that PC1 was biased by a higher lake level and a reduction of material reaching
347 the coring location. Results from the Targo Xian peat bog, located about 16 km east of the southern
348 shore of Tangra Yumco but within its catchment, are in phase with reconstructions from Tangra Yumco
349 as they reveal an onset of wetter conditions at 11.5 cal. ka BP and a further increase in moisture

availability at 11.0 cal. ka BP (Miehe *et al.* 2014). The association of surface runoff with a driving mechanism is more straightforward in the Holocene since glacier fluctuations had probably little effect on the lake level because the glaciers were too small relative to the lake (Rades *et al.* 2013). A modelling study calculated the contribution of glacier meltwater to the total basin runoff as 14% between 2001 and 2011 (Biskop *et al.* 2015). These findings let to the assumption that surface runoff was primarily controlled by precipitation during the Holocene.

After 7.6 cal. ka BP (355 cm ECCD) environmental conditions were rather stable with only minor variations in autochthonous production, i.e., temperature, and surface runoff indicated by only minor variations of TOC, grain sizes, and PC1 (Fig. 3). This interpretation is further confirmed by the lake level reconstructions of Tangra Yumco based on OSL and recalculated cosmogenic nuclide ages that indicate almost constantly falling lake level after the early Holocene (Fig. 6; Ahlborn *et al.* 2016). Data from the Targo Xian peat bog imply drier condition after 7.5 cal. ka BP (Miehe *et al.* 2014) being in phase with the climatic conditions reconstructed for Tangra Yumco.

Palaeoenvironment of the southern Tibetan Plateau

To test, if palaeoenvironmental changes occurred synchronously on the southern Tibetan Plateau, the Tangra Yumco record was compared to records from lakes Nam Co (Kasper *et al.* 2015), Tso Moriri (Mishra *et al.* 2015), and Naleng Co (Figs 1, 6, 7; Opitz *et al.* 2015). Deglaciation and thawing processes started between 17.1 and 16.0 cal. ka BP at Tangra Yumco and Nam Co (Kasper *et al.* 2015) and Tso Moriri (Mishra *et al.* 2015), while conditions at Naleng Co have continuously been cold and dry which is not in phase with results from other records on the southern Tibetan Plateau (Opitz *et al.* 2015). Similar to Tangra Yumco rising temperatures at Nam Co resulted in thawing permafrost and enhanced input of terrestrial TOC (Figs 6, 7; Kasper *et al.* 2015). Lake levels of Tangra Yumco, Nam Co, and Tso Moriri are initially rising (Kasper *et al.* 2015; Mishra *et al.* 2015).

Around 16.0 cal. ka BP Tangra Yumco and Nam Co show a significant shift towards moister conditions (Fig. 6). In the Nam Co record, the pollen association changes from exotic species like *Pinus* and *Picea* to moisture-preferring species like Cyperaceae and Gramineae that is interpreted as a change of the prevailing wind system from a westerly dominance prior to 16.5 cal. ka BP to monsoonal influence thereafter (Zhu *et al.* 2015). This shift is not recorded in sediments from Tso Moriri and delayed or also missing in Naleng Co (Fig. 6). Mishra *et al.* (2015) infer a rising lake level after 16.4 cal. ka BP with

persistent evaporitic conditions due to higher summer insolation. So potential higher moister availability might have been compensated by the evaporitic conditions resulting in the missing signal of monsoonal intensification. At Naleng Co moisture availability increased significantly at 14.8 cal. ka BP (Opitz *et al.* 2015) leaving a temporal offset of approximately 1000 years to monsoonal intensification in Tangra Yumco and Nam Co. However, the chronology of Naleng Co, especially for the Late Pleistocene, suffers from dating uncertainties (Kramer *et al.* 2010) hampering a comparability to other records during this time. Therefore, the reported shifts to moisture conditions around 16.0 cal. ka BP at Tangra Yumco and Nam Co and at 14.8 cal. ka BP at Naleng Co might represent the same event marking the first intensification of monsoonal influence on the southern Tibetan Plateau in the Lateglacial. Progressive warming after approximately 15.0 cal. ka BP was probably favorable for the development of the Indian summer monsoon (An *et al.* 2000) and might be associated with the increase in moisture on the southern Tibetan Plateau around 16.0 cal. ka BP. The driver of the progressive warming and the resultant monsoonal intensification was likely an increase in summer insolation (Berger & Loutre 1991; Kasper *et al.* 2015).

Oscillations in moisture availability and temperature at Tangra Yumco after 13.0 cal. ka BP with moister and warmer conditions prior to 12.4 cal. ka BP followed by drier and cooler conditions between 12.4 and 11.4 cal. ka BP appear synchronously in all records on the southern Tibetan Plateau (Kasper *et al.* 2015; Mishra *et al.* 2015; Opitz *et al.* 2015). Temperature oscillations ($\delta^{18}O$) in the GISP2 ice core from Greenland occur contemporary to variations in temperature in records from the southern Tibetan Plateau (Fig. 7). In the GISP2 ice core these oscillations reflect the Bølling-Allerød and Younger Dryas (Stuiver & Grootes 2000). Kasper *et al.* (2015) and Opitz *et al.* (2015) detected the Bølling-Allerød and Younger Dryas in Nam Co and Naleng Co. The comparison of the records from the southern Tibetan Plateau further supports a coupling of the Asian monsoon system to the Northern Hemisphere climate system prior to the Holocene (Fig. 7).

In all discussed records from the southern Tibetan Plateau a rapid rise in moisture availability around 11.4 cal. ka BP marks the transition to the Holocene (Fig. 6). This rapid rise is accompanied by a rapid increase in temperatures in the records from the southern Tibetan Plateau and the Northern Hemisphere (Fig. 7). At Tangra Yumco moistest and warmest conditions culminate prior to 8.5 ka with a lake level highstand synchronously to highest lake levels in Nam Co at 9.5 cal. ka BP (Kasper *et al.* 2015), highest available moisture at Tso Moriri between 11.2 and 8.5 cal. ka BP (Mishra *et al.* 2015), and moistest and warmest conditions at Naleng Co prior to 8.3 cal. ka BP (Figs 6, 7; Opitz *et al.* 2015).

412 This period represents the Holocene climate optimum that is regarded as the time of maximum
413 postglacial warmth (Winkler & Wang 1993) and coincides with an increase of monsoonal strength
414 between 10.0 and 9.5 cal. ka BP (Overpeck *et al.* 1996). During the middle to late Holocene (after
415 7.6 cal. ka BP) all records show only minor variations with gradually decreasing moisture availability
416 (Fig. 6) suggesting a general aridification on the southern Tibetan Plateau that is widely recorded on the
417 Tibetan Plateau (Van Campo *et al.* 1996; Zhang & Mischke 2009; An *et al.* 2012; Chen *et al.* 2013).

418 Monsoon intensity records from the Arabian Sea and Bay of Bengal reflecting the strength of
419 the Indian summer monsoon show striking similarities with the records from the southern Tibetan
420 Plateau. Monsoonal strength increases in the Bay of Bengal after 15.6 cal. ka BP and in the Arabian
421 Sea at 15.3 cal. ka BP, is higher roughly after 14.6 cal. ka BP, lower after 12.8 cal. ka BP, and increases
422 rapidly at the beginning of the Holocene (Fig. 6; Schulz *et al.* 1998; Rashid *et al.* 2011). The synchronicity
423 of the southern Tibetan Plateau with monsoon intensity records indicates that the palaeohydrology of
424 lakes on the southern Tibetan Plateau was primarily governed by the Indian summer monsoon since
425 approximately 16.0 cal. ka BP when temperatures and lake level at Tangra Yumco initially rose and the
426 pollen association from Nam Co indicated a change from westerly to monsoonal dominance (Zhu *et al.*
427 2015).

428 The comparison of the records from the southern Tibetan Plateau and monsoon intensity
429 records reveals a synchronous pattern of moisture availability on the southern Tibetan Plateau that is
430 governed by variations is monsoon intensity. The influence of previously discussed local peculiarities or
431 geographical settings of the study sites on the palaeohydrology and palaeoenvironment (Mischke *et al.*
432 2008) is neglectable for large lacustrine systems such as the investigated sites on the southern Tibetan
433 Plateau. Inconsistencies between records, earlier leading to the assumption of an asynchronous pattern
434 of moisture availability, can partly be related to coarse-resolution and poorly dated records (Chen *et al.*
435 2008) or unsuitable small lacustrine systems which immediately react to local peculiarities (Ahlborn *et*
436 *al.* 2015). High-resolution records covering the Lateglacial and the Holocene are urgently needed to
437 further assess the spatial and temporal development of moisture availability on the Tibetan Plateau.
438 Previous studies suggested an anti-phase relationship between monsoon and westerly strength
439 modifying their regional extent (An *et al.* 2000, 2012; Vandenberghe *et al.* 2006; Chen *et al.* 2008) and
440 a delimitation of the Indian summer monsoon by mountain barriers on the northern Tibetan Plateau
441 (Ramisch *et al.* 2016) what would result in an asynchronous pattern of moisture availability over the
442 Tibetan Plateau but would not necessarily prove an asynchronous monsoonal development. A thorough

443 comparison of the northern and southern Tibetan Plateau would help to improve the understanding of
444 the anti-phase relationship between monsoon and westerlies, the temporal variability of the northward
445 extension of the Indian summer monsoon, and the impact of mountain ranges.
446
447
448 **Conclusions**
449 The comparison of Tangra Yumco with several lakes along an east-west-transect, namely Nam Co, Tso
450 Moriri, and Naleng Co (Figs 1, 6, 7), reveals a generally synchronous development of moisture
451 availability on the southern Tibetan Plateau. As shown by the synchronicity of the southern Tibetan
452 Plateau and the monsoon intensity records, all four lakes were under the influence of the Indian summer
453 monsoon since at least 16.0 cal. ka BP. A warm and moist period on the southern Tibetan Plateau
454 between 13.0 and 12.4 cal. ka BP is associated with the Bølling-Allerød, whereas the period between
455 12.4 cal. ka BP and the onset of the Holocene is marked by cooler and drier conditions reflecting the
456 Younger Dryas. After a rapid increase in moisture availability and temperature at the transition to the
457 Holocene, the Holocene climate optimum occurs prior to approximately 8.5 cal. ka BP on the southern
458 Tibetan Plateau. Summarizing, our study supports a spatial and temporal synchronous development of
459 the Indian summer monsoon with a neglectable influence of local peculiarities or geographical settings
460 of the studied large lake systems.
461
462
463 *Acknowledgements.* – This work is part of the Sino-German collaboration within the DFG priority
464 program 1372 “TiP – Tibetan Plateau: Formation–Climate–Ecosystem” (Grant No. MA1308/23-2) and
465 is jointly financed by the National Natural Science Foundation of China (Grant No. 41271225). We
466 gratefully acknowledge the help of Nico Blaubach, Kati Hartwig, and Carmen Kirchner with analyses
467 and of Willi Ackermann, Martin Lederer, Thomas Reuss, and Sascha Schröter with sample pretreatment.
468 We thank Jaques Labrie for providing a modified version of the GRADISTAT software. Stephan Opitz
469 and Sushma Prasad are acknowledged for their kind cooperation. The manuscript markedly benefited
470 from the thorough review of Andy Henderson. Karoline Henkel and Thomas Kasper thank the Max
471 Planck Society and the Carl-Zeiss-Stiftung for the funding of their Ph.D. grants.
472
473

References

Ahlborn, M., Haberzettl, T., Wang, J., Alivernini, M., Schlütz, F., Schwarz, A., Su, Y., Frenzel, P., Daut, G., Zhu, L. & Mäusbacher, R. 2015: Sediment dynamics and hydrologic events affecting small lacustrine systems on the southern-central Tibetan Plateau – the example of TT Lake. *The Holocene 25*, 508-522.

Ahlborn, M., Haberzettl, T., Wang, J., Fürstenberg, S., Mäusbacher, R., Mazzocco, J., Pierson, J., Zhu, L. & Frenzel, P. 2016: Holocene lake level history of the Tangra Yumco lake system, southern-central Tibetan Plateau. *The Holocene 26*, 176-187.

Akita, L. G., Frenzel, P., Haberzettl, T., Kasper, T., Wang, J. & Reicherter, K. 2015: Ostracoda (Crustacea) as indicators of subaqueous mass movements: An example from the large brackish lake Tangra Yumco on the southern Tibetan Plateau, China. *Palaeogeography, Palaeoclimatology, Palaeoecology 419*, 60-74.

An, Z., Colman, S. M., Zhou, W., Li, X., Brown, E. T., Jull, A. J. T., Cai, Y., Huang, Y., Lu, X., Chang, H., Song, Y., Sun, Y., Xu, H., Liu, W., Jin, Z., Liu, X., Cheng, P., Liu, Y., Ai, L., Li, X., Liu, X., Yan, L., Shi, Z., Wang, X., Wu, F., Qiang, X., Dong, J., Lu, F. & Xu, X. 2012: Interplay between the Westerlies and Asian monsoon recorded in Lake Qinghai sediments since 32 ka. *Scientific Reports 2*, 1-7.

An, Z., Porter, S. C., Kutzbach, J. E., Wu, X., Wang, S., Liu, X., Li, X. & Zhou, W. 2000: Asynchronous Holocene optimum of the East Asian monsoon. *Quaternary Science Reviews 19*, 743-762.

Berger, A. & Loutre, M. F. 1991: Insolation values for the climate of the last 10 million years. *Quaternary Science Reviews 10*, 297-317.

Biskop, S., Maussion, F., Krause, P. & Fink, M. 2015: What are the key drivers of regional differences in the water balance on the Tibetan Plateau? *Hydrology & Earth System Sciences Discussions 12*, 4271-4314.

Blott, S. J. & Pye, K. 2001: GRADISTAT: A grain size distribution and statistics package for the analysis of unconsolidated sediments. *Earth Surface Processes and Landforms 26*, 1237-1248.

Brunschön, C., Haberzettl, T. & Behling, H. 2010: High-resolution studies on vegetation succession, hydrological variations, anthropogenic impact and genesis of a subrecent lake in southern Ecuador. *Vegetation History and Archaeobotany 19*, 191-206.

Chen, F., Yu, Z., Yang, M., Ito, E., Wang, S., Madsen, D. B., Huang, X., Zhao, Y., Sato, T., Birks, H. J. B., Boomer, I., Chen, J., An, C. & Wünnemann, B. 2008: Holocene moisture evolution in arid central Asia and its out-of-phase relationship with Asian monsoon history. *Quaternary Science Reviews 27*, 351-364.

Chen, Y., Zong, Y., Li, B., Li, S. & Aitchison, J. C. 2013: Shrinking lakes in Tibet linked to the weakening Asian monsoon in the past 8.2 ka. *Quaternary Research 80*, 189-198.

Croudace, I. W., Rindby, A. & Rothwell, R. G. 2006: ITRAX: description and evaluation of a new multi-function X-ray core scanner. *In* Rothwell, R. G. (ed.): *New Techniques in Sediment Core Analysis*, 51-63. Geological Society, London, 267.

Daut, G., Mäusbacher, R., Baade, J., Gleixner, G., Kroemer, E., Mügler, I., Wallner, J., Wang, J. & Zhu, L. 2010: Late Quaternary hydrological changes inferred from lake level fluctuations of Nam Co (Tibetan Plateau, China). *Quaternary International 218*, 86–93.

Dietze, E., Hartmann, K., Diekmann, B., IJmker, J., Lehmkuhl, F., Opitz, S., Stauch, G., Wünnemann, B. & Borchers, A. 2012: An end-member algorithm for deciphering modern detrital processes from lake sediments of Lake Donggi Cona, NE Tibetan Plateau, China. *Sedimentary Geology 243–244*, 169-180.

Dietze, E., Maussion, F., Ahlborn, M., Diekmann, B., Hartmann, K., Henkel, K., Kasper, T., Lockot, G., Opitz, S. & Haberzettl, T. 2014: Sediment transport processes across the Tibetan Plateau inferred from robust grain-size end members in lake sediments. *Climate of the Past 10*, 91-106.

Doberschütz, S., Frenzel, P., Haberzettl, T., Kasper, T., Wang, J., Zhu, L., Daut, G., Schwalb, A. & Mäusbacher, R. 2014: Monsoonal forcing of Holocene paleoenvironmental change on the central Tibetan Plateau inferred using a sediment record from Lake Nam Co (Xizang, China). *Journal of Paleolimnology 51*, 253-266.

Dong, J., Wang, Y., Cheng, H., Hardt, B., Edwards, R. L., Kong, X., Wu, J., Chen, S., Liu, D., Jiang, X. & Zhao, K. 2010: A high-resolution stalagmite record of the Holocene East Asian monsoon from Mt Shennongjia, central China. *The Holocene 20*, 257-264.

Feng, Z.-D., An, C. B. & Wang, H. B. 2006: Holocene climatic and environmental changes in the arid and semi-arid areas of China: a review. *The Holocene 16*, 119-130.

533 Haberzettl, T. 2015: Advances in Limnogeology and Paleolimnology. *Habilitation thesis*, *Friedrich*
534 *Schiller University Jena*, 36 pp., http://nbn-resolving.de/urn:nbn:de:gbv:27-20160107-133023-
535 6.
536 Haberzettl, T., Anselmetti, F. S., Bowen, S. W., Fey, M., Mayr, C., Zolitschka, B., Ariztegui, D., Mauz,
537 B., Ohlendorf, C., Kastner, S., Lücke, A., Schäbitz, F. & Wille, M. 2009: Late Pleistocene dust
538 deposition in the Patagonian steppe - extending and refining the paleoenvironmental and
539 tephrochronological record from Laguna Potrok Aike back to 55 ka. *Quaternary Science*
540 *Reviews 28*, 2927-2939.
541 Haberzettl, T., Henkel, K., Kasper, T., Ahlborn, M., Su, Y., Wang, J., Appel, E., St-Onge, G., Stoner,
542 J., Daut, G., Zhu, L. & Mäusbacher, R. 2015: Independently dated paleomagnetic secular
543 variation records from the Tibetan Plateau. *Earth and Planetary Science Letters 416*, 98-108.
544 He, Y., Theakstone, W. H., Zhang, Z., Zhang, D., Yao, T., Chen, T., Shen, Y. & Pang, H. 2004:
545 Asynchronous Holocene climatic change across China. *Quaternary Research 61*, 52- 63.
546 Henkel, K., Haberzettl, T., St-Onge, G., Wang, J., Ahlborn, M., Daut, G., Zhu, L. & Mäusbacher, R.
547 2016: High-resolution paleomagnetic and sedimentological investigations on the Tibetan
548 Plateau for the past 16 ka cal B.P.—The Tangra Yumco record. *Geochemistry, Geophysics,*
549 *Geosystems 17*, 774-790.
550 Herzschuh, U. 2006: Palaeo-moisture evolution in monsoonal Central Asia during the last 50,000
551 years. *Quaternary Science Reviews 25*, 163-178.
552 Hudson, A. M. & Quade, J. 2013: Long-term east-west asymmetry in monsoon rainfall on the Tibetan
553 Plateau. *Geology 41*, 351-354.
554 Kasper, T., Frenzel, P., Haberzettl, T., Schwarz, A., Daut, G., Meschner, S., Wang, J., Zhu, L. &
555 Mäusbacher, R. 2013: Interplay between redox conditions and hydrological changes in
556 sediments from Lake Nam Co (Tibetan Plateau) during the past 4000 cal BP inferred from
557 geochemical and micropaleontological analyses. *Palaeogeography, Palaeoclimatology,*
558 *Palaeoecology 392*, 261-271.
559 Kasper, T., Haberzettl, T., Doberschütz, S., Daut, G., Wang, J., Zhu, L., Nowaczyk, N. & Mäusbacher,
560 R. 2012: Indian Ocean Summer Monsoon (IOSM)-dynamics within the past 4 ka recorded in
561 the sediments of Lake Nam Co, central Tibetan Plateau (China). *Quaternary Science Reviews*
562 *39*, 73-85.
563 Kasper, T., Haberzettl, T., Wang, J., Daut, G., Doberschütz, S., Zhu, L. & Mäusbacher, R. 2015:
564 Hydrological variations on the Central Tibetan Plateau since the Last Glacial Maximum and
565 their teleconnection to inter-regional and hemispheric climate variations. *Journal of Quaternary*
566 *Science 30*, 70-78.
567 Kemp, A. L. W., Thomas, R. L., Wong, H. K. T. & Johnston, L. M. 1977: Nitrogen and C/N ratios in the
568 sediments of Lakes Superior, Huron, St. Clair, Erie, and Ontario. *Canadian Journal of Earth*
569 *Sciences 14*, 2402-2413.
570 Kong, P., Na, C., Brown, R., Fabel, D., Freeman, S., Xiao, W. & Wang, Y. 2011: Cosmogenic ^{10}Be and
571 ^{26}Al dating of paleolake shorelines in Tibet. *Journal of Asian Earth Sciences 41*, 263-273.
572 Kramer, A., Herzschuh, U., Mischke, S. & Zhang, C. 2010: Late glacial vegetation and climate
573 oscillations on the southeastern Tibetan Plateau inferred from the Lake Naleng pollen profile.
574 *Quaternary Research 73*, 324-335.
575 Krishnamurthy, R. V., Bhattacharya, S. K. & Kusumgar, S. 1986: Palaeoclimatic changes deduced
576 from ^{13}C/^{12}C and C/N ratios of Karewa lake sediments, India. *Nature 323*, 150-152.
577 Lockot, G., Ramisch, A., Wünnemann, B., Hartmann, K., Haberzettl, T., Chen, H. & Diekmann, B.
578 2015: A process- and provenance-based attempt to unravel inconsistent radiocarbon
579 chronologies in lake sediments – an example from Lake Heihai, North Tibetan Plateau
580 (China). *Radiocarbon 57*, 1003-1019.
581 Long, H., Haberzettl, T., Tsukamoto, S., Shen, J., Kasper, T., Daut, G., Zhu, L., Mäusbacher, R. &
582 Frechen, M. 2015: Luminescence dating of lacustrine sediments from Tangra Yumco
583 (southern Tibetan Plateau) using post-IR IRSL signals from polymineral grains. *Boreas 44*,
584 139-152.
585 Long, H., Lai, Z., Frenzel, P., Fuchs, M. & Haberzettl, T. 2012: Holocene moist period recorded by the
586 chronostratigraphy of a lake sedimentary sequence from Lake Tangra Yumco on the south
587 Tibetan Plateau. *Quaternary Geochronology 10*, 136-142.
588 Maussion, F., Scherer, D., Mölg, T., Collier, E., Curio, J. & Finkelnburg, R. 2014: Precipitation
589 Seasonality and Variability over the Tibetan Plateau as Resolved by the High Asia Reanalysis.
590 *Journal of Climate 27*, 1910-1927.
591 Meyers, P. A. & Ishiwatari, R. 1993: Lacustrine organic geochemistry—an overview of indicators of
592 organic matter sources and diagenesis in lake sediments. *Organic Geochemistry 20*, 867-900.

593 Miehe, S., Miehe, G., van Leeuwen, J. F. N., Wrozyna, C., van der Knaap, W. O., Duo, L. &
594 Haberzettl, T. 2014: Persistence of *Artemisia* steppe in the Tangra Yumco Basin, west-central
595 Tibet, China: despite or in consequence of Holocene lake-level changes? *Journal of*
596 *Paleolimnology 51*, 267-285.
597 Mischke, S., Kramer, M., Zhang, C., Shang, H., Herzschuh, U. & Erzinger, J. 2008: Reduced early
598 Holocene moisture availability in the Bayan Har Mountains, northeastern Tibetan Plateau,
599 inferred from a multi-proxy lake record. *Palaeogeography, Palaeoclimatology, Palaeoecology*
600 *267*, 59-76.
601 Mischke, S., Weynell, M., Zhang, C. & Wiechert, U. 2013: Spatial variability of ^{14}C reservoir effects in
602 Tibetan Plateau lakes. *Quaternary International 313–314*, 147-155.
603 Mischke, S. & Zhang, C. 2010: Holocene cold events on the Tibetan Plateau. *Global and Planetary*
604 *Change 72*, 155-163.
605 Mishra, P. K., Anoop, A., Schettler, G., Prasad, S., Jehangir, A., Menzel, P., Naumann, R., Yousuf, A.
606 R., Basavaiah, N., Deenadayalan, K., Wiesner, M. G. & Gaye, B. 2015: Reconstructed late
607 Quaternary hydrological changes from Lake Tso Moriri, NW Himalaya. *Quaternary*
608 *International 371*, 76-86.
609 Mügler, I., Gleixner, G., Günther, F., Mäusbacher, R., Daut, G., Schütt, B., Berking, J., Schwalb, A.,
610 Schwark, L., Xu, B., Yao, T., Zhu, L. & Yi, C. 2010: A multi-proxy approach to reconstruct
611 hydrological changes and Holocene climate development of Nam Co, Central Tibet. *Journal of*
612 *Paleolimnology 43*, 625-648.
613 Nakagawa, T. 2007: Double-L channel: an amazingly non-destructive method of continuous sub-
614 sampling from sediment cores. *Quaternary International 298*, 167-168 (Supplement).
615 Opitz, S., Zhang, C., Herzschuh, U. & Mischke, S. 2015: Climate variability on the south-eastern
616 Tibetan Plateau since the Lateglacial based on a multiproxy approach from Lake Naleng –
617 comparing pollen and non-pollen signals. *Quaternary Science Reviews 115*, 112-122.
618 Overpeck, J., Anderson, D., Trumbore, S. & Prell, W. 1996: The southwest Indian Monsoon over the
619 last 18 000 years. *Climate Dynamics 12*, 213-225.
620 Peng, Y., Xiao, J., Nakamura, T., Liu, B. & Inouchi, Y. 2005: Holocene East Asian monsoonal
621 precipitation pattern revealed by grain-size distribution of core sediments of Daihai Lake in
622 Inner Mongolia of north-central China. *Earth and Planetary Science Letters 233*, 467-479.
623 Pye, K. & Tsoar, H. 2009: *Aeolian Sand and Sand Dunes*. 458 pp. Springer, Berlin.
624 Rades, E. F., Hetzel, R., Xu, Q. & Ding, L. 2013: Constraining Holocene lake-level highstands on the
625 Tibetan Plateau by ^{10}Be exposure dating: a case study at Tangra Yumco, southern Tibet.
626 *Quaternary Science Reviews 82*, 68-77.
627 Rades, E. F., Tsukamoto, S., Frechen, M., Qiang, X. & Lin, D. 2015: A lake-level chronology based on
628 feldspar luminescence dating of beach ridges at the Tangra Yum Co (southern Tibet).
629 *Quaternary Research 83*, 469-478.
630 Ramisch, A., Lockot, G., Haberzettl, T., Hartmann, K., Kuhn, G., Lehmkuhl, F., Schimpf, S., Schulte,
631 P., Stauch, G., Wang, R., Wünnemann, B., Yan, D., Zhang, Y. & Diekmann, B. 2016: A
632 persistent northern boundary of Indian Summer Monsoon precipitation over Central Asia
633 during the Holocene. *Scientific Reports 6*, 1-7.
634 Rashid, H., England, E., Thompson, L. & Polyak, L. 2011: Late Glacial to Holocene Indian Summer
635 Monsoon Variability Based upon Sediment Records Taken from the Bay of Bengal. *Terrestrial,*
636 *Atmospheric and Oceanic Sciences 22*, 215-228.
637 Reimer, P. J., Bard, E., Bayliss, A., Beck, J. W., Blackwell, P. G., Ramsey, C. B., Buck, C. E., Cheng,
638 H., Edwards, R. L. & Friedrich, M. 2013: IntCal13 and Marine13 radiocarbon age calibration
639 curves 0–50,000 years cal BP. *Radiocarbon 55*, 1869-1887.
640 Schulz, H., von Rad, U. & Erlenkeuser, H. 1998: Correlation between Arabian Sea and Greenland
641 climate oscillations of the past 110,000 years. *Nature 393*, 54-57.
642 Sletten, K., Blikra, L. H., Ballantyne, C. K., Nesje, A. & Dahl, S. O. 2003: Holocene debris flows
643 recognized in a lacustrine sedimentary succession: sedimentology, chronostratigraphy and
644 cause of triggering. *The Holocene 13*, 907-920.
645 Stanton, T., Snowball, I., Zillén, L. & Wastegård, S. 2010: Validating a Swedish varve chronology
646 using radiocarbon, palaeomagnetic secular variation, lead pollution history and statistical
647 correlation. *Quaternary Geochronology 5*, 611-624.
648 Stuiver, M. & Grootes, P. M. 2000: GISP2 Oxygen Isotope Ratios. *Quaternary Research 53*, 277-284.
649 Stuiver, M. & Reimer, P. J. 1993: Radiocarbon Calibration Program, Calib Rev 6.0.0. *Radiocarbon 35*,
650 215-230.
651 Su, Y., Gao, X., Liu, Q., Hu, P., Duan, Z., Jiang, Z., Wang, J., Zhu, L., Doberschütz, S., Mäusbacher,
652 R., Daut, G. & Haberzettl, T. 2013: Mechanism of variations in environmental magnetic

proxies of lake sediments from Nam Co, Tibet during the Holocene. *Chinese Science Bulletin 58*, 1568-1578.

Sun, D., Bloemendal, J., Rea, D. K., Vandenberghe, J., Jiang, F., An, Z. & Su, R. 2002: Grain-size distribution function of polymodal sediments in hydraulic and aeolian environments, and numerical partitioning of the sedimentary components. *Sedimentary Geology 152*, 263-277.

Van Campo, E., Cour, P. & Hang, S. 1996: Holocene environmental changes in Bangong Co basin (Western Tibet). Part 2: The pollen record. *Palaeogeography, Palaeoclimatology, Palaeoecology 120*, 49-63.

Vandenberghe, J., Renssen, H., van Huissteden, K., Nugteren, G., Konert, M., Lu, H., Dodonov, A. & Buylaert, J.-P. 2006: Penetration of Atlantic westerly winds into Central and East Asia. *Quaternary Science Reviews 25*, 2380-2389.

Wang, J., Peng, P., Ma, Q. & Zhu, L. 2010a: Modern limnological features of Tangra Yumco and Zhari Namco, Tibetan Plateau. *Journal of Lake Sciences 22*, 629-632.

Wang, J., Zhu, L., Wang, Y., Ju, J., Daut, G. & Li, M. 2015: Spatial variability and the controlling mechanisms of surface sediments from Nam Co, central Tibetan Plateau, China. *Sedimentary Geology 319*, 69-77.

Wang, Y., Liu, X. & Herzschuh, U. 2010b: Asynchronous evolution of the Indian and East Asian Summer Monsoon indicated by Holocene moisture patterns in monsoonal central Asia. *Earth-Science Reviews 103*, 135-153.

Wang, Y., Zhu, L., Wang, J., Ju, J. & Lin, X. 2012: The spatial distribution and sedimentary processes of organic matter in surface sediments of Nam Co, Central Tibetan Plateau. *Chinese Science Bulletin 57*, 4753-4764.

Winkler, M. G. & Wang, P. K. 1993: The late-Quaternary vegetation and climate of China. *In* Wright Jr., H. E., Kutzbach, J. E., Webb, T., Ruddiman, W. F., Street-Perrott, F. A. & Bartlein, P. J. (eds.): *Global climates since the last glacial maximum*, 221-264. University of Minnesota Press, Minneapolis.

Wischnewski, J., Mischke, S., Wang, Y. & Herzschuh, U. 2011: Reconstructing climate variability on the northeastern Tibetan Plateau since the last Lateglacial – a multi-proxy, dual-site approach comparing terrestrial and aquatic signals. *Quaternary Science Reviews 30*, 82-97.

Yang, Q., Jochum, K. P., Stoll, B., Weis, U., Börner, N., Schwalb, A., Frenzel, P., Scholz, D., Doberschütz, S., Haberzettl, T., Gleixner, G., Mäusbacher, R., Zhu, L. & Andreae, M. O. 2014: Trace element variability in single ostracod valves as a proxy for hydrochemical change in Nam Co, central Tibet, during the Holocene. *Palaeogeography, Palaeoclimatology, Palaeoecology 399*, 225-235.

Zhang, C. & Mischke, S. 2009: A Lateglacial and Holocene lake record from the Nianbaoyeze Mountains and inferences of lake, glacier and climate evolution on the eastern Tibetan Plateau. *Quaternary Science Reviews 28*, 1970-1983.

Zhu, L., Lü, X., Wang, J., Peng, P., Kasper, T., Daut, G., Haberzettl, T., Frenzel, P., Li, Q., Yang, R., Schwalb, A. & Mäusbacher, R. 2015: Climate change on the Tibetan Plateau in response to shifting atmospheric circulation since the LGM. *Scientific Reports 5*, 1-8.

Zhu, L., Wu, Y., Wang, J., Lin, X., Ju, J., Xie, M., Li, M., Mäusbacher, R., Schwalb, A. & Daut, G. 2008: Environmental changes since 8.4 ka reflected in the lacustrine core sediments from Nam Co, central Tibetan Plateau, China. *The Holocene 18*, 831-839.

Figure captions

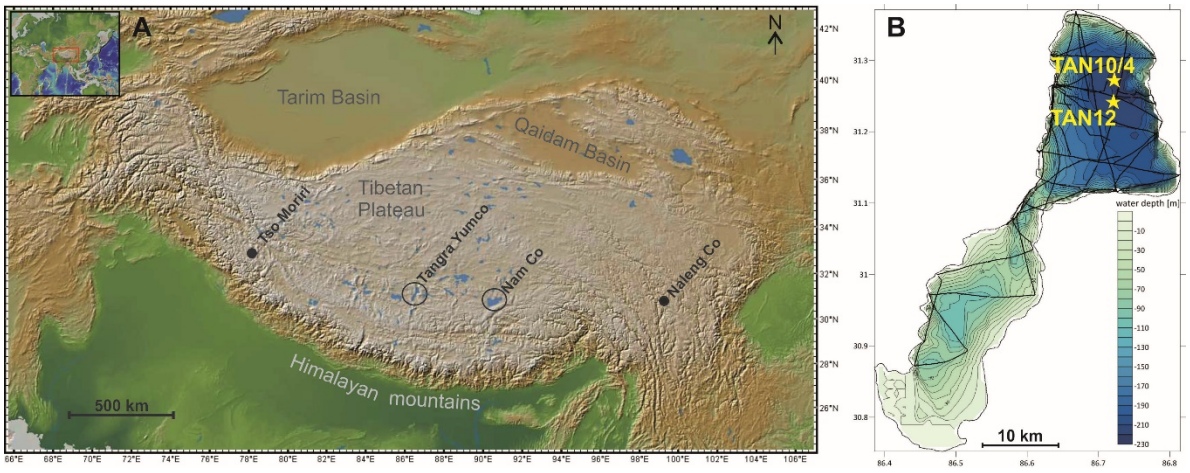

Fig. 1. Study site. A. Map of the Tibetan Plateau with Tangra Yumco (circle), Nam Co (circle), Tso Moriri (dot), and Naleng Co (dot). Source: http://www.geomapapp.org. B. Bathymetric map of Tangra Yumco with sampling location of cores TAN10/4 and TAN12 (stars) with tracks of hydro-acoustic survey (black lines).

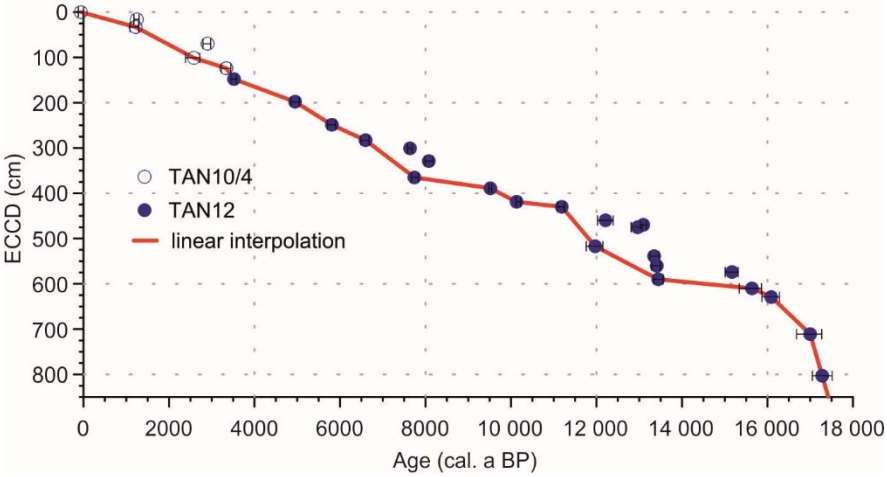

Fig. 2. Chronology of record TAN12 as published in Henkel *et al.* (2016). A change in sedimentation rate occurs around at 16.0 cal. ka BP. The sedimentation rate is 3.6 mm a^{-1} below 711 cm ECCD (17.1 cal. ka BP) and with <0.6 mm a^{-1} significantly lower above.

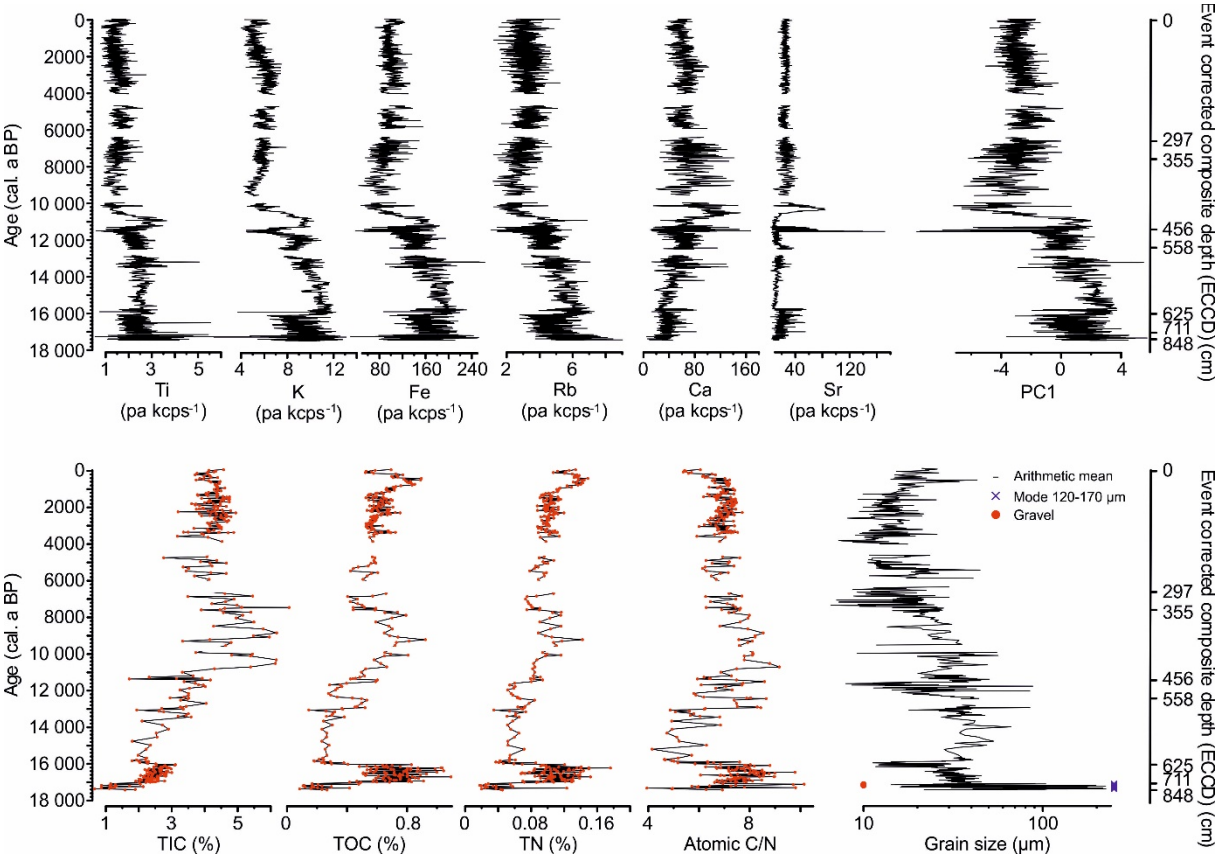

709

710 *Fig. 3.* Results of XRF (2 mm resolution), PC1 representing the surface runoff, CNS analyses (<10 cm
711 resolution), and grain size analyses (1 cm resolution) on a logarithmic scale. Discontinuity of the plots
712 is due to data gaps between core sections.

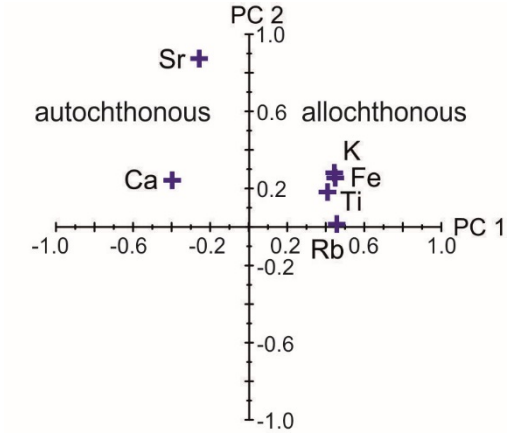

713

714 *Fig. 4.* Results of the principle component analysis. The PC1 accounts for 63.06% while PC2 accounts
715 for 14.43% of the total variance and basically represents Sr. PC1 is considered to reflect the
716 allochthonous clastic input as it has high accounts of K, Ti, Fe, and Rb.

717

718

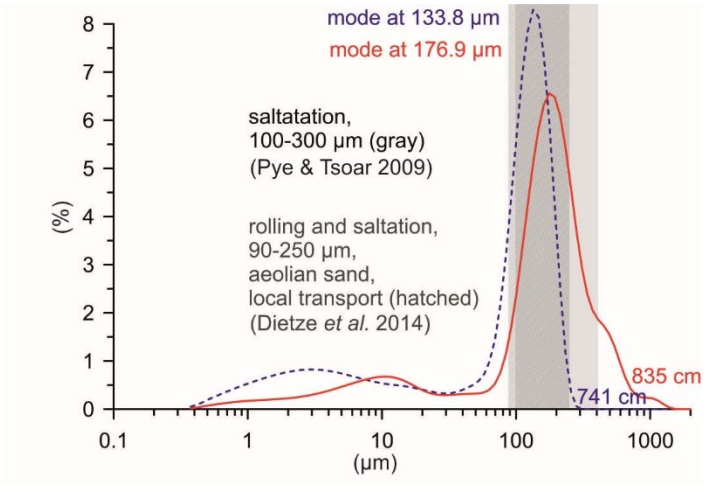

719

720 *Fig. 5.* Grain size distribution of sand layers prior to 17.1 cal. ka BP. Layer at 835 cm ECCD
721 (17.5 cal. ka BP; red bold) has a mode at 176.9 µm. Layer at 741 cm ECCD (17.1 cal. ka BP; blue
722 dashed) has a mode at 133.8 µm. Unimodal distribution and good sorting indicates aeolian transport.
723 Rolling and saltation happens to grains with a size of 90–250 µm (hatched; Dietze *et al.* 2014) or 100–
724 300 µm (gray; Pye & Tsoar 2009).

725

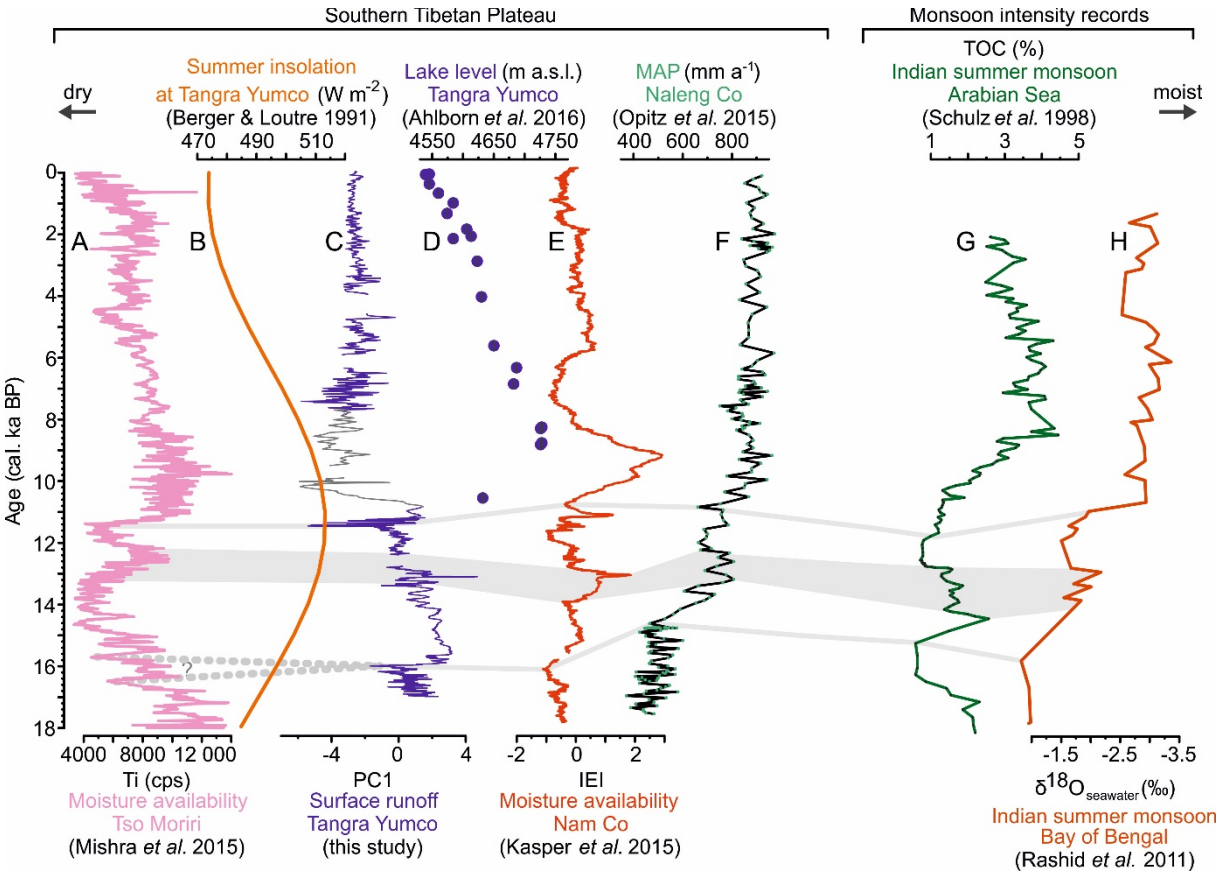

Fig. 6. Comparison of clastic input of (A) Tso Moriri (Mishra *et al.* 2015), (B) summer insolation at Tangra Yumco (Berger & Loutre 1991), (C) PC1 representing the surface runoff of Tangra Yumco, gray interval is biased by either dilution effect of the carbonate production or higher lake level and a reduction of material reaching the coring location and do, therefore, not represent the surface runoff (discontinuity of the plot is due to data gaps between core sections), (D) lake level curve of Tangra Yumco (blue dots; Ahlborn *et al.* 2016), (E) inflow–evaporation index of Nam Co (IEI; Kasper *et al.* 2015), (F) mean annual precipitation (MAP) of Naleng Co based on a pollen transfer function (Opitz *et al.* 2015), (G) Indian monsoon record from the Arabian Sea (Schulz *et al.* 1998), and (H) Indian monsoon record from the Bay of Bengal (Rashid *et al.* 2011). Indicated with gray bars are synchronous shifts as the increase in moisture availability around 16.0 cal. ka BP, enhanced moisture after 13.0 cal. ka BP, and the increase in moisture availability around 11.4 cal. ka BP.

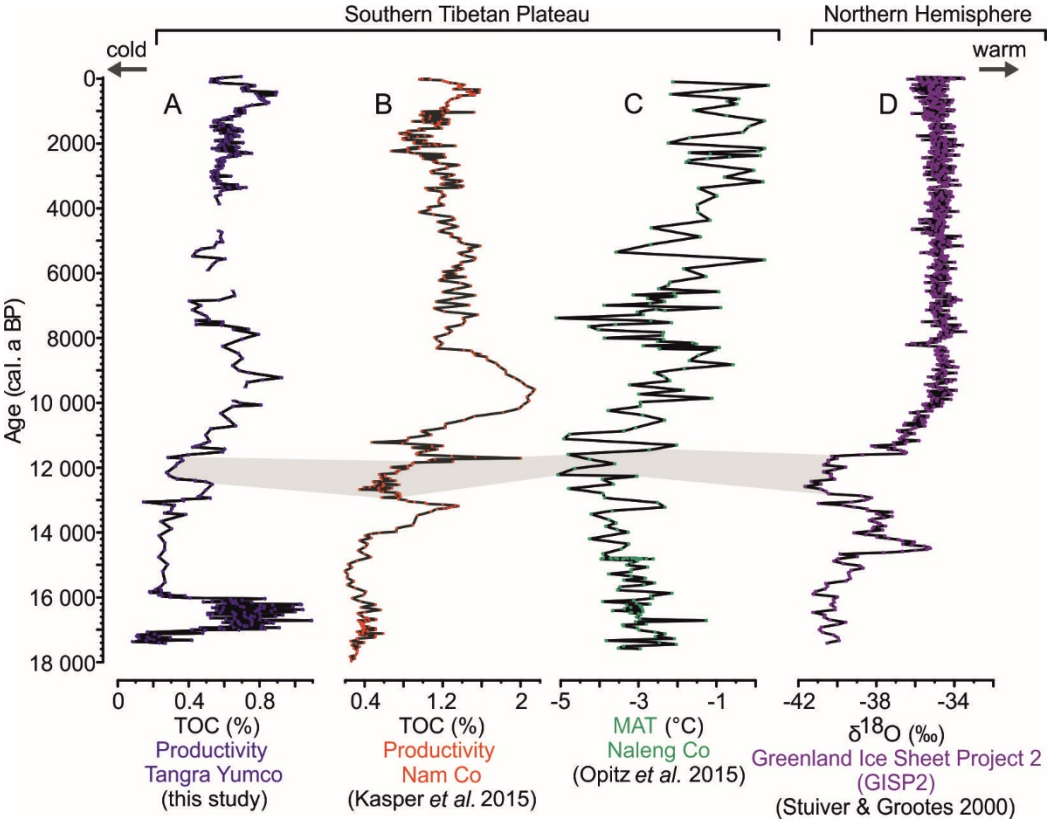

Fig. 7. Indicators for temperature variations from the southern Tibetan Plateau. A. TOC as indicator for biological productivity of Tangra Yumco (this study, discontinuity of the plots is due to data gaps between core sections). B. TOC as indicator for biological productivity of Nam Co (Kasper *et al.* 2015). C. Mean annual temperature (MAT) of Naleng Co based on a pollen transfer function (Opitz *et al.* 2015). D. $\delta^{18}O$ from the GISP2 ice core from Greenlandas temperature indicator for the Northern Hemisphere (Stuiver & Grootes 2000). Indicated with a gray bar is a decline in temperature in the records from the southern Tibetan Plateau and the Northern Hemisphere prior to the onset of the Holocene associated with the Younger Dryas preceded by enhanced temperatures of the Bølling-Allerød.